Current Optics and Photonics
Vol. 3, No. 3, June 2019, pp. 199-203

ISSN: 2508-7266(Print) / ISSN: 2508-7274(Online)
DOI: https://doi.org/10.3807/COPP.2019.3.3.199

Analysis of a Photonic Crystal Fiber Sensor with Reuleaux Triangle

Pibin Bing[1]*, Shichao Huang[1], Xinyue Guo[1], Hongtao Zhang[1], Lian Tan[1], Zhongyang Li[1], and Jianquan Yao[1,2]

[1]*College of Electric Power, North China University of Water Resources and Electric Power, Zhengzhou, Henan 450045, China*
[2]*College of Precision Instruments and Opto-Electronic Engineering, Institute of Laser and Opto-electronics, Tianjin University, Tianjin 300072, China*

(Received December 4, 2018 : revised May 8, 2019 : accepted May 8, 2019)

The characteristics of a photonic crystal fiber sensor with reuleaux triangle are studied by using the finite element method. The wavelength sensitivity of the designed optical fiber sensor is related to the arc radius of the reuleaux triangle. Whether the core area is solid or liquid as well as the refractive index of the liquid core contributes to wavelength sensitivity. The simulation results show that larger arc radius leads to higher sensitivity. The sensitivity can be improved by introducing a liquid core, and higher wavelength sensitivity can be achieved with a lower refractive index liquid core. In addition, the specific channel plated with gold film is polished and then analyte is deposited on the film surface, in which case the position of the resonance peak is the same as that of the complete photonic crystal fiber with three analyte channels being filled with analyte. This means that filling process becomes convenient with equivalent performance of designed sensor. The maximum wavelength sensitivity of the sensor is 10200 nm/RIU and the resolution is 9.8×10^{-6} RIU.

Keywords : Photonic crystal fiber, Wavelength sensitivity, Liquid core
OCIS codes : (060.2370) Fiber optics sensors; (060.2280) Fiber design and fabrication; (060.2270) Fiber characterization

I. INTRODUCTION

Photonic crystal fiber (PCF) has a promising application in system integration and remote sensing [1] due to its small size, high sensitivity and flexible design [2]. It can be used as an ultrabroad bandwidth polarization filter [3], optical sensor [4], filters [5, 6], power beam combiner [7], splitters [8, 9], and surface plasmon resonance (SPR) sensor [10]. The PCF sensor based on SPR solves the problem of phase matching and liquid filling into an optical fiber sensor [11]. These crucial virtues have aroused wide attention in recent years. Large detection range [12], high sensitivity [13] and high linearity [14] optical fiber sensors have been designed and reported. In addition, PCF sensors can be used to detect temperature [15, 16]. To be used as a multiplex sensor has also been investigated. For instance, it can detect temperature and magnetic field [17] or temperature and refractive index (RI) [18]. The index guided photonic crystal fiber (IG-PCF) sensors can be designed as suspended core structure [19], grapefruit shaped structure [20], elliptical air hole structure [21] and the like, which each is applied to various detection conditions for its own advantages. The diversity of PCF sensors with new structure means different PCF sensing devices can be chosen for specific demands. For example, the D-shaped photonic crystal fiber sensors simplify the coating and filling difficulty [22-24], and a sensor with Indium Tin Oxide can be used to detect in the near infrared region [25, 26].

In this paper, a photonic crystal fiber sensor with reuleaux triangle is proposed and the influence of the parameters on the designed sensor is studied. The numerical simulation results show that higher wavelength sensitivity

*Corresponding author: bing463233@163.com, ORCID 0000-0003-0059-135X
Color versions of one or more of the figures in this paper are available online.

is obtained with larger arc radius of the reuleaux triangle. The wavelength sensitivity of the PCF sensor with liquid core is larger than with solid core. In addition, the sensitivity of the sensor with lower RI liquid core is larger than that with higher RI liquid core. Further analysis shows that the position of the resonance peak has no change when the analyte channel coated with gold film is polished, which means that the polished structure facilitates analyte filling without affecting the sensitivity. The maximum wavelength sensitivity of the sensor is 10200 nm/RIU and the resolution is 9.8×10^{-6} RIU.

II. DESIGN AND ANALYSIS

The schematic of the photonic crystal fiber sensor with reuleaux triangle is shown as Fig. 1(a). Small holes are in hexagonal arrangement inside the reuleaux triangle. The space of Λ is 2 μm. The diameters of the small holes are $d_1 = 0.6\Lambda$, and the RI of liquid core is $n_c = 1.40$. Three analyte channels are numbered 1~3 anticlockwise. Each channel consists of a fraction of reuleaux triangular curve near the core and circular curve far from the core (see in Fig. 1(a)). Therein, the arc radius of the reuleaux triangle is $L = 3.3\Lambda$ and the radius of the circle is 8 μm. The strut between two adjacent large channels has two small air holes with $d_2 = 0.6\Lambda$. The thickness of the strut and gold film are 0.8Λ and 40 nm, respectively. The dielectric constant of gold is given by the Drude model [10]. The outermost layer is a perfect matching layer (PML). Positions and dimensions of every component in rectangular coordinates are drawn in Fig. 1(b). The material of the photonic crystal fiber (background material) is SiO_2, and its refractive index is given by the Sellmeier equation [27]. The refractive index of the analyte (n) varies from 1.33 to 1.39.

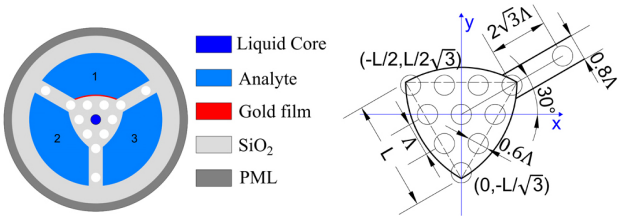

(a) (b)

FIG. 1. (a) Schematic of the designed sensor; (b) Positions and dimensions of every component in rectangular coordinates.

Figure 2(a) is the dispersion relationships of the core mode and the plasma mode at n = 1.38. At the phase matching point (λ_{res} = 802 nm), the energy in the core mode is strongly transferred to the plasma mode. The difference of the two real parts of the effective refractive index (n_{eff}) becomes larger far away from the phase matching point. Synchronously, the energy transferred to the film-analyte interface becomes smaller (as illustrated in Fig. 2(a)).

According to Ref. [27], confinement loss is defined as:

$$\alpha(dB/m) = 40\pi \times Im(n_{eff})/\ln(10)\lambda \quad (1)$$

where λ is the wavelength of the incident light.

The confinement loss curves are shown in Fig. 2(b) with n changing from 1.33 to 1.39. The effective refractive index of the plasma mode (red curve in Fig. 2(a)) increases when the refractive index of the analyte increases, leading to a red shift of the resonance peak. The increase of resonance peak intensity indicates that the mode coupling increases with the increase of n. However, as is shown in Fig. 2(b), the resonance peak intensity at n = 1.39 is not significantly increased comparing to n = 1.38. The shape of this curve at n = 1.39 is also different from other confinement loss curve. This is because the curved surface plated with gold film supports several plasmonic peaks [10], and the second peaks are closer to the first peak. On

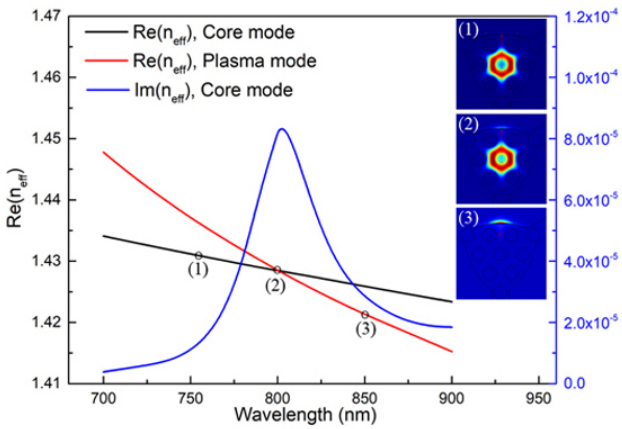

(a)

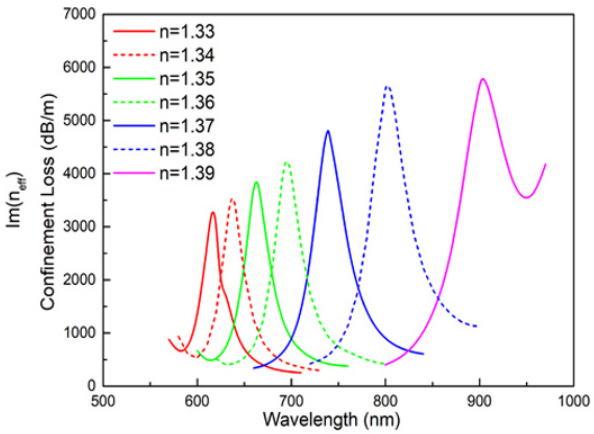

(b)

FIG. 2. (a) Dispersion relationships of the core mode (black and blue curves) and the surface plasmon (red curve) at n = 1.38; (b) Confinement loss with n varying from 1.33 to 1.39.

the one hand, two adjacent resonance peaks make the curve more identifiable due to its own feature. On the other hand, it may be difficult to judge peak displacement when the distance is small.

The wavelength sensitivity is calculated as in Ref. [23]:

$$S_\lambda(nm/RIU) = \Delta\lambda_{peak}/\Delta n_a \quad (2)$$

where $\Delta\lambda_{peak}$ is the displacement of the resonance peak, and Δn_a is the change of the analyte.

The detectable index resolution is defined according to Ref. [23]:

$$R(RIU) = \Delta\lambda_{\min}\Delta n/\Delta\lambda_{res} = \Delta\lambda_{\min}/S_\lambda \quad (3)$$

where $\Delta\lambda_{min}$ is the spectral minimum resolution.

The resonance peak has a redshift with the RI of analyte increasing. When the refractive index changes from 1.38 to 1.39, the displacement of the resonance peak is 102 nm. The maximum wavelength sensitivity of the sensor is 10200 nm/RIU by Eq. (2), and the resolution (R) is 9.8×10^{-6} RIU assuming $\Delta\lambda_{min} = 0.1$ nm.

III. RESULTS AND DISCUSSION

In order to study the influence of arc radius as well as the core on wavelength sensitivity, the relationships between the RI of analyte and wavelength sensitivity with solid core and liquid core are drawn in Fig. 3. The refractive index of the liquid core is $n_c = 1.40$. It shows that the wavelength sensitivity of the PCF sensor with liquid core is larger than that with solid core at the same arc radius condition. It is because the refractive index of the liquid is lower than that of SiO_2. So, the effective refractive index of PCF is lower, which is closer to the refractive index of analyte, strengthening mode coupling. Resonance peak intensity and wavelength sensitivity get larger accordingly. Therefore, liquid core PCF has more advantages in sensitivity than solid core PCF. When discussing the impact of arc radius on the sensitivity of the sensor, L is larger than 2.9Λ to prevent the small hole structure of the hexagon from being destroyed by the reuleaux triangle area. In this paper, L is set to 2.9Λ, 3.1Λ and 3.3Λ. As in Fig. 3, the larger the arc radius, the greater the sensitivity. The larger arc radius means smaller curvature, so the secondary peak has less impact on the primary resonance peak. It is extremely conducive to coating as well as even coating that a larger arc radius parameter is adopted. It should be pointed out that liquid core is formed by filling liquid into the central hole. Although higher sensitivity can be obtained by introducing liquid core, it is still difficult to encapsulate liquid into the central hole. If liquid is replaced by solid material with a refractive index of 1.40, the performance is the same.

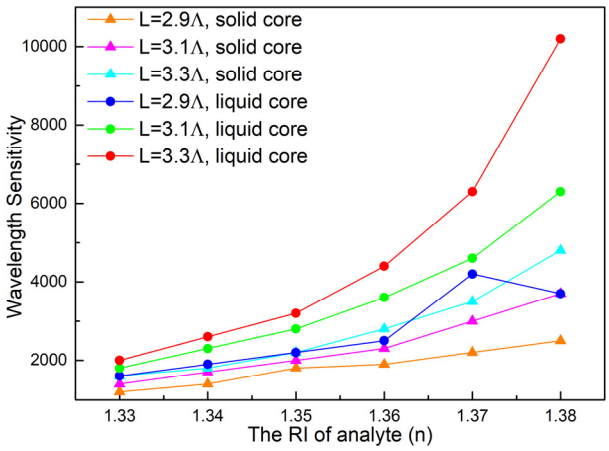

FIG. 3. Influence of different arc radius on wavelength sensitivity of sensor with solid core and liquid core.

The confinement loss and resonance wavelength of the sensor are affected by the RI of liquid core (n_c). The loss curves at different n_c are shown in Fig. 4(a) for $n = 1.38$ and $n = 1.39$. Resonance peak intensity is smaller at higher RI of the liquid core. The decrease of resonance peak intensity is due to greater RI of the liquid core. More energy is confined by the liquid core, leading to the decrease of the leaked energy to the gold film surface. Thus, the intensity decreases. In Fig. 4(b), Three real part curves of the effective RI with different liquid core appear significantly different. The larger the RI of the liquid core, the larger the real part value of effective RI of the core mode. Also, the resonance wavelength shows a blue shift. The blueshift is cause by an increase of effective RI of the core mode for its larger liquid core so that the phase matching point shifts toward shorter wavelength. High wavelength sensitivity can be obtained and detection range is 1.33~1.39 when the RI of the liquid core is 1.40. From Figs. 4(a) and 4(b), what can be known is that the resonance peak intensity and wavelength sensitivity are greater when the refractive index of the liquid core is smaller. However, increasing wavelength sensitivity is at the expense of reducing the dynamic range of refractive index detection. Obviously, in order to maintain a larger detection range, a small RI value of the liquid core is not suitable. The refractive index of the liquid core is selected as 1.40 in this paper.

Generally, gold film plated on analyte channel is rather difficult, and the process of filling analyte with the capillary effect is not convenient. It deserves to be explored whether the sensitivity will be affected if the photonic crystal fiber with the reuleaux triangle is polished. Analyte channel numbered 1 in Fig. 1(a) is polished, and the other analyte channels have no analyte. The analyte is only placed on the metallized surface of the No.1 channel that has been polished. The confinement loss curves (solid curves) with PCF not being polished at $n = 1.33$, $n = 1.35$, $n = 1.37$ and

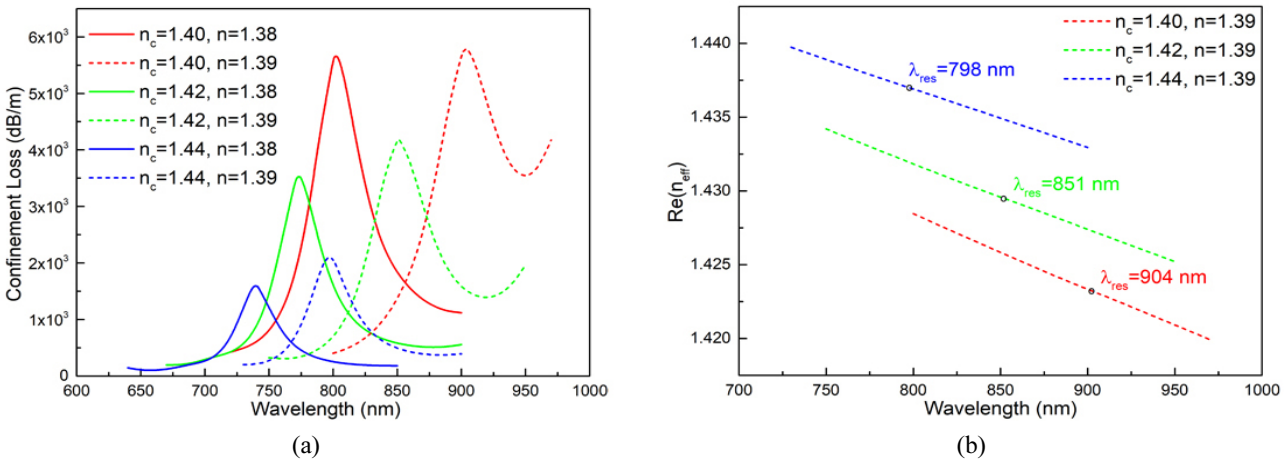

(a) (b)

FIG. 4. (a) Confinement loss curves at different n_c for n = 1.38 and n = 1.39; (b) Real part curves of the effective refractive index with different liquid core at n = 1.39.

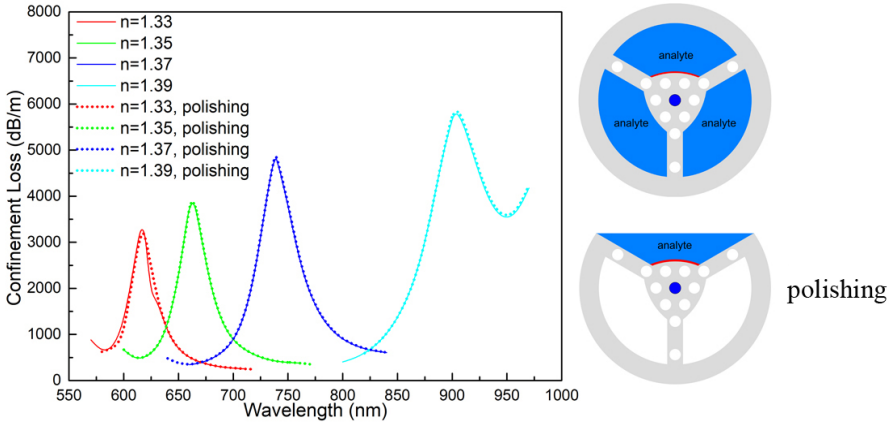

FIG. 5. Confinement loss curves with PCF polished and not being polished (The schematic of the two types is attached in the right).

n = 1.39 as well as those curves with PCF being polished (dotted curves) are drawn in Fig. 5. It shows confinement loss curves almost coincide at the same RI condition, and the position of the two resonance peaks is the same. Therefore, the two types share the same relation curves between refractive index and resonance wavelength so that both of them are the red curve in Fig. 3. It is easy to understand that the surface plasmon resonance occurs at the interface between gold film and analyte, and plasmon at other channels with no gold film is not existent. Whether the channel is filled with analyte or not does not affect resonance wavelength and influence on the intensity of the resonance peak is negligible, which means equal performance is acquired and the difficulty of coating gold film and depositing analyte is reduced by polishing the metallized channel rather than by coating the inside of the air hole as in ref. [12]. The wavelength sensitivity of the sensor can reach to 10200 nm/RIU, which is higher than that of the sensors when it is coated with gold film on the outer surface in ref. [28] and ref. [29]. The sensor with reuleaux triangle can save more coating materials. The polished PCF sensor has the advantage of simplifying fabrication, making it desirable for applications.

IV. CONCLUSION

The characteristics of a photonic crystal fiber sensor with reuleaux triangle are numerically simulated. The arc radius of the reuleaux triangle, whether solid core or liquid core and the refractive index of the liquid core, have an impact on wavelength sensitivity of the PCF sensor. The larger arc radius can achieve higher wavelength sensitivity. Compared to the sensor with solid core, the sensitivity can be improved by introducing a liquid core. The lower the refractive index of the liquid core, the higher the sensitivity. In addition, the channels free of gold film have no effect on the resonance peak. Polishing the channel which is coated with gold film and then depositing analyte on the film can simplify the filling process. The maximum wavelength sensitivity of the designed sensor is 10200 nm/RIU, and the resolution is 9.8×10^{-6} RIU.

ACKNOWLEDGMENT

This work was supported by the National Natural Science Foundation of China (Grant Nos. 61601183, 61675147, and 61735010), the National Key Research and Development Program of China (Grant No. 2017YFA0700202), and the Graduate Education Innovation Program Fund of North China University of Water Resources and Electric Power (Grant No. YK2017-04).

REFERENCES

1. N. N. Luan, R. Wang, W. H. Lv, and J. Q. Yao, "Surface plasmon resonance sensor based on D-shaped microstructured optical fiber with hollow core," Opt. Express **23**, 8576-8582 (2015).
2. X. C. Yang, Y. Lu, B. L. Liu, and J. Q. Yao, "Temperature sensor based on photonic crystal fiber filled with liquid and silver nanowires," IEEE Photonics J. **8**, 6803309 (2016).
3. H. L. Chen, S. G. Li, M. J. Ma, Z. K. Fan, and Y. D. Wu, "Ultrabroad bandwidth polarization filter based on D-shaped photonic crystal fibers with gold film," Plasmonics **10**, 1239-1242 (2015).
4. K. Li, M. Jiang, Z. Z. Zhao, and Z. M. Wang, "Low coherence technique to interrogate optical sensors based on selectively filled double-core photonic crystal fiber for temperature measurement," Opt. Commun. **389**, 234-238 (2017).
5. S. H. Zhang, J. S. Li, S. G. Li, Q. Liu, Y. C. Liu, Z. Zhang, and Y. J. Wang, "A tunable single-polarization photonic crystal fiber filter based on surface plasmon resonance," Appl. Phys. B **124**, 112 (2018).
6. X. Zhou, S. G. Li, T. L. Cheng, and G. W. An, "Design of offset core photonic crystal fiber filter based on surface plasmon resonance," Opt. Quantum Electron. **50**, 157 (2018).
7. D. Malka, E. Cohen, and Z. Zalevsky, "Design of 4×1 power beam combiner based on multicore photonic crystal fiber," Appl. Sci.-Basel **7**, 695 (2017).
8. D. Malka and Z. Zalevsky, "Multicore photonic crystal fiber based 1×8 two-dimensional intensity splitters/couplers," Electromagnetics **33**, 413-420 (2013).
9. D. Malka and A. Peled, "Power splitting of 1×16 in multicore photonic crystal fibers," Appl. Surf. Sci. **417**, 34-39 (2017).
10. A. Hassani and M. Skorobogatiy, "Design criteria for microstructured-optical-fiber-based surface-plasmon-resonance sensors," J. Opt. Soc. Am. B **24**, 1423-1429 (2007).
11. A. Hassani and M. Skorobogatiy, "Design of the micro-structured optical fiber-based surface plasmon resonance sensors with enhanced microfluidics," Opt. Express **14**, 11616-11621 (2006).
12. B. B. Shuai, L. Xia, Y. T. Zhang, and D. M. Liu, "A multi-core holey fiber based plasmonic sensor with large detection range and high linearity," Opt. Express **20**, 5974-5986 (2012).
13. X. C. Yang, Y. Lu, M. T. Wang, and J. Q. Yao, "SPR sensor based on exposed-core grapefruit fiber with bimetallic structure," IEEE Photonics Technol. Lett. **28**, 649-652 (2016).
14. F. M. Wang, Z. J. Sun, C. Liu, T. Sun, and P. K. Chu, "A highly sensitive dual-core photonic crystal fiber based on a surface plasmon resonance biosensor with silver-graphene layer," Plasmonics **12**, 1847-1853 (2017).
15. C. Liu, F. M. Wang, J. W. Lv, T. Sun, Q. Liu, C. F. Fu, H. W. Mu, and P. K. Chu, "A highly temperature-sensitive photonic crystal fiber based on surface plasmon resonance," Opt. Commun. **359**, 378-382 (2016).
16. W. Xu, J. Q. Yao, X. C. Yang, J. Shi, J. F. Zhao, and C. Zhang, "Analysis of hollow fiber temperature sensor filled with graphene-ag composite nanowire and liquid," Sensors **16**, 1656 (2016).
17. X. G. Li, X. Zhou, Y. Zhao, and R. Q. Lv, "Multi-modes interferometer for magnetic field and temperature measurement using Photonic crystal fiber filled with magnetic fluid," Opt. Fiber Technol. **41**, 1-6 (2018).
18. N. N. Luan and J. Q. Yao, "Refractive index and temperature sensing based on surface plasmon resonance and directional resonance coupling in a PCF," IEEE Photonics J. **9**, 1-8 (2017).
19. J. Pniewski, A. Ramaniuk, R. Kasztelanic, M. Śmietana, M. Trippenbach, and R. Buczyński, "Applicability of suspended-core fibres for attenuation-based label-free biosensing," Opt. Commun. **402**, 290-295 (2017).
20. X. C. Yang, Y. Lu, M. T. Wang, and J. Q. Yao, "An exposed-core grapefruit fibers based surface plasmon resonance sensor," Sensors **15**, 17106-17114 (2015).
21. E. K. Akowuah, T. Gorman, H. Ademgil, S. Haxha, G. K. Robinson, and J. V. Oliver, "Numerical analysis of a photonic crystal fiber for biosensing applications," IEEE J. Quantum Electron. **48**, 1403-1410 (2012).
22. M. Tian, P. Lu, L. Chen, C. Lv, and D. M. Liu, "All-solid D-shaped photonic fiber sensor based on surface plasmon resonance," Opt. Commun. **285**, 1550-1554 (2012).
23. G. W. An, S. Li, W. Qin, W. Zhang, Z, K. Fan, and Y. J. Bao, "High-sensitivity refractive index sensor based on D-Shaped photonic crystal fiber with rectangular lattice and nanoscale gold film," Plasmonics **9**, 1355-1360 (2014).
24. C. Liu, W. Q. Su, Q. Liu, X. L. Lu, F. M. Wang, T. Sun, and P. K. Chu, "Symmetrical dual D-shape photonic crystal fibers for surface plasmon resonance sensing," Opt. Express **26**, 9039-9049 (2018).
25. J. N. Dash and R. Jha, "SPR biosensor based on polymer PCF coated with conducting metal oxide," IEEE Photonics Technol. Lett. **26**, 595-598 (2014).
26. J. N. Dash and R. Jha, "Highly sensitive D shaped PCF sensor based on SPR for near IR," Opt. Quantum Electron. **48**, 137 (2016).
27. R. K. Gangwar and V. K. Singh, "Highly sensitive surface plasmon resonance based D-shaped photonic crystal fiber refractive index sensor," Plasmonics **12**, 1367-1372 (2017).
28. M. R. Momota and M. R. Hasan, "Hollow-core silver coated photonic crystal fiber plasmonic sensor," Opt. Mater. **76**, 287-294 (2018).
29. S. Chakma, M. A. Khalek, B. K. Paul, K. Ahmed, M. R. Hasan, and A. N. Bahara, "Gold-coated photonic crystal fiber biosensor based on surface plasmon resonance: Design and analysis," Sens. Biosensing Res. **18**, 7-12 (2018).